

## B-D-Xylosidase from *Selenomonas ruminantium*: Catalyzed Reactions with Natural and Artificial Substrates

Douglas B. Jordan

Received: 5 May 2007 / Accepted: 26 September 2007 /  
Published online: 17 October 2007  
© Humana Press Inc. 2007

**Abstract** Catalytically efficient  $\beta$ -D-xylosidase from *Selenomonas ruminantium* (SXA) exhibits  $pK_{a,s}$  5 and 7 (assigned to catalytic base, D14, and catalytic acid, E186) for  $k_{cat}/K_m$  with substrates 1,4- $\beta$ -D-xylobiose (X2) and 1,4- $\beta$ -D-xylotriose (X3). Catalytically inactive, dianionic SXA (D14<sup>-</sup>E186<sup>-</sup>) has threefold lower affinity than catalytically active, monoanionic SXA (D14<sup>-</sup>E186<sup>H</sup>) for X2 and X3, whereas D14<sup>-</sup>E186<sup>-</sup> has twofold higher affinity than D14<sup>-</sup>E186<sup>H</sup> for 4-nitrophenyl- $\beta$ -D-xylopyranoside (4NPX), and D14<sup>-</sup>E186<sup>-</sup> has no affinity for 4-nitrophenyl- $\alpha$ -L-arabinofuranoside. Anomeric isomers,  $\alpha$ -D-xylose and  $\beta$ -D-xylose, have similar affinity for SXA. 4-Nitrophenol competitively inhibits SXA-catalyzed hydrolysis of 4NPX. SXA steady-state kinetic parameters account for complete progress curves of SXA-catalyzed hydrolysis reactions.

**Keywords** Fuel ethanol · Glycoside hydrolase · GH43 · Hemicellulose · pH dependence · Stereochemistry · Inhibitor · Assay method

### Introduction

B-D-Xylosidase/ $\alpha$ -L-arabinofuranosidase from the ruminal anaerobic bacterium *Selenomonas ruminantium* (SXA) is a bifunctional glycoside hydrolase possessing  $\beta$ -D-xylosidase activity (EC 3.2.1.37) and  $\alpha$ -L-arabinofuranosidase activity (EC 3.2.1.55) [1–3]. Its amino acid sequence places SXA within glycoside hydrolase family 43 (GH43) and structural clan F in the CAZy database (carbohydrate active enzymes database, <http://www.cazy.org/>) [4, 5]. Because of its exceptionally efficient catalysis of xylooligosaccharide hydrolysis [3], its arabinofuranosidase function for cleaving arabinose side chains from arabinoxylooligosac-

---

The mention of firm names or trade products does not imply that they are endorsed or recommended by the U.S. Department of Agriculture over other firms or similar products not mentioned.

D. B. Jordan (✉)

Fermentation Biotechnology Research Unit, National Center for Agricultural Utilization Research, U.S. Department of Agriculture, Agricultural Research Service, 1815 N. University Street, Peoria, IL 61604, USA

e-mail: douglas.jordan@ars.usda.gov

charides [1], and its good stability properties [2], SXA has potential utility in industrial processes where it could serve double duty in depolymerizing complex carbohydrates (i.e., arabinoxylans) of herbaceous biomass to simple sugars for subsequent fermentation to fuel ethanol and other bioproducts [6–9]. In this regard, it is particularly important, from an efficiency viewpoint, to engage a catalytically powerful  $\beta$ -D-xylosidase in saccharification of xylans: for example, even in an all-enzymatic saccharification process, the  $\beta$ -D-xylosidase would be required to catalyze hydrolysis of more glycosidic bonds than other enzymes in the process (e.g.,  $\beta$ -xylanases that cleave larger polymers of D-xylose, xylans, to xylooligosaccharides), and benefits of the process cannot fully be realized until this ultimate step of saccharification is complete.

X-ray structures have been determined for GH43  $\beta$ -xylosidases isolated from *Bacillus subtilis*, *Bacillus halodurans*, *Clostridium acetobutylicum*, and *Geobacillus stearothermophilus*, which have 53–70% protein sequence identity with SXA [3, 10]. The structures describe homotetrameric proteins with monomers comprising two domains: an N-terminal, five-bladed  $\beta$ -propeller domain that contains the two-subsite, funnel-shaped active site, which has a single route for access by ligands; and a C-terminal  $\beta$ -sandwich domain that serves to restrict the size of the active site. Structures of catalytically impaired mutant enzymes from *G. stearothermophilus* in complex with 1,4- $\beta$ -D-xylobiose [10] are highly useful for modeling ligands in the active site of SXA, particularly as the eight amino acid residues in the vicinity of the xylose moiety of the nonreducing end of xylobiose, which occupy subsite -1, are fully conserved in SXA.

Structure–function studies have secured that SXA catalyzes hydrolysis of substrates with inversion of anomeric stereochemistry, implicating a single transition state with the catalytic base (D14) serving to activate a water molecule for addition to substrate and the catalytic acid (E186) serving to protonate the leaving group [3]; SXA catalyzes the hydrolysis of a single residue from the nonreducing end of the substrate without processivity so that all products of the hydrolysis reaction are removed from the active site before initiating another catalytic cycle [3]; and the  $\beta$ -xylosidase and  $\alpha$ -arabinofuranosidase activities share the single active site of the SXA protomer [3].

Besides the determination that 4NPX is tenfold faster than 4NPA as substrate for SXA [3], there are additional differences between the competing substrates (Fig. 1). Similar to 4NPX, SXA-catalyzed hydrolysis of 4NPA proceeds with inversion of anomeric stereochemistry. However, unlike the  $\alpha$ -D-xylose product of the SXA-catalyzed hydrolysis of 4NPX, which has a half-life of  $\sim 1$  h for mutarotation (Fig. 1a), the  $\beta$ -L-arabinofuranose product of SXA-catalyzed hydrolysis of 4NPA more rapidly undergoes mutarotation and ring reorganization to arabinopyranose, which dominates at equilibrium [3]. Secondly, whereas catalytically inactive, dianionic SXA (D14<sup>-</sup>E186<sup>-</sup>) forms a dead end, binary complex with 4NPX that has a twofold tighter binding constant than the productive complex comprising catalytically active, monoanionic SXA (D14<sup>-</sup>E186<sup>H</sup>) and 4NPX (Fig. 1b), SXA in the dianionic form does not bind 4NPA [3]. Thirdly, whereas 4NPX forms a ternary, inhibited complex (SXA-D-xylose-4NPX), 4NPA does not [11]. In this work, pH profiles of steady-state kinetic parameters for SXA-catalyzed hydrolysis of 1,4- $\beta$ -D-xylobiose (X2) and 1,4- $\beta$ -D-xylotriose (X3) are determined for comparison with those of 4NPX and 4NPA and analyzing the affinity of catalytically inactive D14<sup>-</sup>E186<sup>-</sup> SXA for the natural substrates. SXA affinities for D-xylose preparations enriched in  $\alpha$ -D-xylose or  $\beta$ -D-xylose content are determined to assess whether SXA recognizes its reaction product ( $\alpha$ ) better than its anomeric isomer. The affinity of 4-nitrophenol for SXA is determined to assess whether its inhibition constant needs to be included in describing SXA-catalyzed hydrolysis of 4NPX. Lastly, an improved procedure is established for quenching SXA-

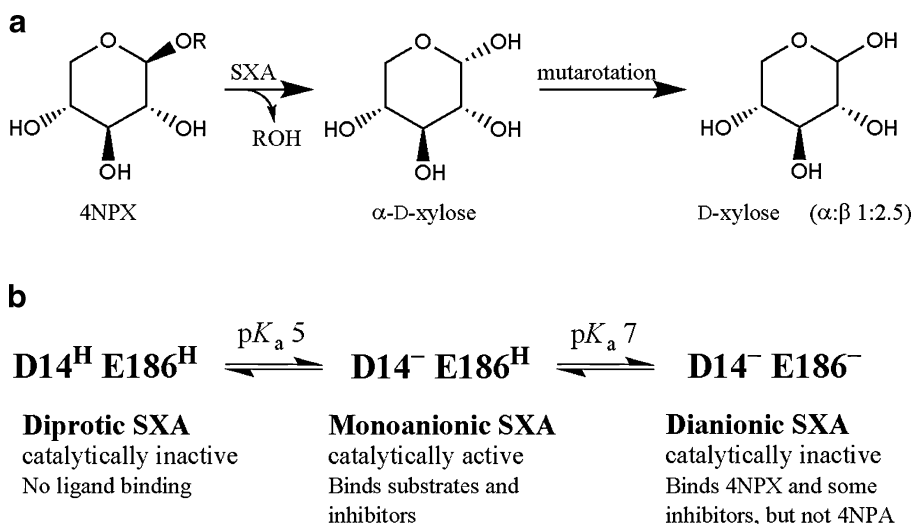


**Fig. 1** Properties of SXA-catalyzed hydrolysis of 4-nitrophenyl- $\beta$ -D-xylopyranoside (4NPX). **a** Stereochemistry. SXA catalyzes hydrolysis of 4NPX with inversion of anomeric configuration. Mutarotation, off the enzyme, converts  $\alpha$ -D-xylose to its equilibrium mixture ( $\alpha$ : $\beta$  ratio of 1:2.5) with a half-life of  $\sim$ 1 h [3].  $R = 4$ -nitrophenyl. **b** Diprotic model.  $\text{p}K_{\text{a}}$ s 5 and 7, assigned to catalytic base (D14) and catalytic acid (E186), respectively, govern catalysis and binding of ligands [3]

catalyzed reactions for high performance liquid chromatography (HPLC) analysis of products.

## Materials and Methods

### Materials and General Methods

Buffers, 4-nitrophenol (4NP), 4-nitrophenyl- $\beta$ -D-xylopyranoside (4NPX), 4-nitrophenyl- $\alpha$ -L-arabinofuranoside (4NPA), and D-xylose (X1) were obtained from Sigma-Aldrich (St. Louis, MO). 1,4- $\beta$ -D-Xylobiose (X2), 1,4- $\beta$ -D-xylotriose (X3), 1,4- $\beta$ -D-xylotetraose (X4), 1,4- $\beta$ -D-xylopentaose (X5), and 1,4- $\beta$ -D-xylohexaose (X6) were from Megazyme (Wicklow, Ireland). Water was purified through a Milli-Q unit (Millipore; Billerica, MA). All other reagents were reagent grade and high purity. The gene encoding  $\beta$ -xylosidase from *S. ruminantium* GA192 was cloned and expressed in *Escherichia coli* as described [1]. SXA, produced in *E. coli*, was purified to homogeneity, as judged from sodium dodecyl sulfate-polyacrylamide gel electrophoresis (SDS-PAGE) analysis, by using reverse phase and anionic exchange chromatography steps as described [3] with the addition of a final desalting, gel filtration step employing a  $2.6 \times 30$  cm column of Bio-Gel P-6 DG desalting gel (Bio-Rad; Hercules, CA), equilibrated and developed with 20 mM sodium phosphate, pH 7.0. Concentrations of homogeneous SXA protomers (active sites) were determined by using an extinction coefficient at 280 nm of  $129,600 \text{ M}^{-1} \text{ cm}^{-1}$ , calculated from amino acid composition [3, 12]. A Cary 50 Bio UV-Visible spectrophotometer (Varian; Palo Alto, CA), equipped with a thermostatted holder for cuvettes, was used for spectral and kinetic determinations. A model SX.18MV-R stopped-flow (Applied Photophysics; Leatherhead, UK) with a thermostatted compartment for syringes and reaction chamber and a 2-mm path length for absorbance measurements was used for rapid kinetic studies. Kinetic simulations

were through the computer program KINSIM: Chemical Kinetics Simulation System, 32-bit DOS-Extended Version 4.0, March 1997 [13]. Delta extinction coefficients (product–substrate) at 360, 380, and 400 nm were determined for each buffer condition by subtracting the molar absorbance of 4NPX from that of 4-nitrophenol (4NP) [3]. The concentration of 4NP was determined by using the published extinction coefficient of  $18.3 \text{ mM}^{-1}\text{cm}^{-1}$  at 400 nm for 4NP in NaOH [14]. Concentrations of 4NPX and 4NPA were determined by incubating substrate with excess enzyme until an end point was reached, adding an aliquot (10–100  $\mu\text{l}$ ) to 0.99–0.90 ml 0.1 M NaOH, recording the absorbance at 400 nm and using the extinction coefficient of  $18.3 \text{ mM}^{-1}\text{cm}^{-1}$  for 4NP in NaOH.

### HPLC Analysis of Reactions

Products from SXA-catalyzed hydrolysis of substrates X2–X6 and 4NPX were separated and quantified by using a DX500 HPLC system with an ED40 electrochemical detector (pulsed amperometry), AS3500 autosampler, PA-100 ( $4 \times 250 \text{ mm}$ ) anion exchange column, and Chromeleon software (Dionex, Sunnyvale, CA). Samples (25  $\mu\text{l}$ ) were injected onto the column equilibrated with 0.1 M NaOH and developed with a 5-min linear gradient (0.1 M NaOH to 33 mM sodium acetate) at  $\sim 25^\circ\text{C}$  and a flow rate of  $1 \text{ ml min}^{-1}$ . Several concentrations of the products of interest (e.g., D-xylose and X2) were used to establish standard curves on the same day experimental samples were run. Substrate concentrations were determined by HPLC analysis of samples incubated with excess SXA for complete conversion to D-xylose.

### Kinetics with Substrates X2–X6

For determination of steady-state kinetic parameters of X2–X6 substrates, 0.5-ml reaction mixtures contained varied substrate concentrations (0.9–13 mM) in 100 mM succinate–NaOH, pH 5.3 at  $25^\circ\text{C}$ . For pH studies of SXA-catalyzed hydrolysis of X2 and X3, buffers of constant ionic strength ( $I=0.3 \text{ M}$ ), adjusted with NaCl, were used as indicated (replacing 100 mM succinate–NaOH, pH 5.3): 100 mM succinate–NaOH (pH 4.3–6), 100 mM sodium phosphate (pH 6–8), and 30 mM sodium pyrophosphate (pH 8–9.2). Before (time = 0 min) and after (time = 0.5–2 min) initiating reactions with enzyme (7  $\mu\text{l}$  SXA in 20 mM sodium phosphate, pH 7.0), 100- $\mu\text{l}$  aliquots of reaction mixtures were removed and quenched with an equal volume of 0.2 M sodium phosphate pH 11.3 at  $0^\circ\text{C}$  (so that quenched mixtures were pH 10.5–11) and diluted by adding 1 mM sodium phosphate, pH 10.5–11 at  $0^\circ\text{C}$  as necessary (typically 200–800  $\mu\text{l}$  added to 200  $\mu\text{l}$  quenched samples) to adjust concentrations of reactants and products to fall within the linear range of standard curves. Samples were kept on wet ice or the HPLC autosampler at  $5^\circ\text{C}$  until analyzed by HPLC. Initial rates, calculated from linear regressions of the [D-xylose] produced vs time, were fitted to Eq. 1 to determine steady-state kinetic parameters. Parameter,  $k_{\text{cat}}$ , is expressed in moles of substrate hydrolyzed per second per mole enzyme active sites (protomers); thus, for substrate X2, the [D-xylose] produced was divided by two to provide the [X2] hydrolyzed, whereas for X3–X6, the [D-xylose] produced was taken as the concentration of substrate hydrolyzed.

### Reaction Progress Curves

For X2, 2-ml reactions contained 100 mM succinate–NaOH, pH 5.3 at  $25^\circ\text{C}$ . Concentrations of SXA (protomer) and X2 are indicated in the figure legends. Before

(time=0) and after initiating reactions with enzyme (7  $\mu\text{l}$  SXA in 20 mM sodium phosphate, pH 7.0), 100- $\mu\text{l}$  aliquots of reaction mixtures were removed, quenched with an equal volume of 0.2 M sodium phosphate pH 11.3 at 0°C, and diluted with 1 mM sodium phosphate, pH 10.5–11 (as above) before HPLC analysis.

For 4NPX, 1.5-ml reactions contained 100 mM succinate–NaOH, pH 5.3 at 25°C and concentrations of 4NPX and SXA (protomer) as indicated in the figure legends. Before (time=0) and after initiating reactions with enzyme (7  $\mu\text{l}$  SXA in 20 mM sodium phosphate, pH 7.0), 10–100  $\mu\text{l}$  aliquots of reaction mixtures were removed and added to cuvettes containing 900–990  $\mu\text{l}$  0.1 M NaOH (final volume=1,000  $\mu\text{l}$ ); absorbencies at 400 nm were recorded and converted to molarities by using the extinction coefficient of 18.3  $\text{mM}^{-1} \text{cm}^{-1}$  for 4NP in NaOH [14].

### Determination of Inhibition Constants

For D-xylose inhibition of SXA-catalyzed hydrolysis of 4NPX, 1-ml reactions contained varied concentrations (0.2–7 mM) of 4NPX and varied concentrations (0, 20, 60, and 150 mM) of D-xylose in 100 mM succinate–NaOH, pH 5.3 at 25°C. Reactions were initiated by adding enzyme (7  $\mu\text{l}$  SXA in 20 mM sodium phosphate, pH 7.0), and reaction progress was monitored continuously for 0.3 min at 380 nm to determine initial rates (fitted to lines). For determination of steady-state kinetic parameters, initial rates were fitted to Eq. 2 (competitive inhibition) and Eq. 3 (noncompetitive inhibition).

For inhibition of SXA-catalyzed hydrolysis of 4NPA by two D-xylose preparations having different ratios of  $\alpha$  and  $\beta$  anomeric isomers, the stopped-flow instrument was used to allow rapid execution of three to five replicates for each reaction condition. The experiment relies on the experimentally determined production of  $\alpha$ -D-xylose from SXA-catalyzed hydrolysis of 4NPX and 1,4- $\beta$ -D-xylose (X2), the experimentally determined half-life ( $\sim 1$  h) of  $\alpha$ -D-xylose mutarotation to its equilibrium position ( $\alpha$ : $\beta$  ratio of 1:2.5), and the experimentally determined  $\alpha$ : $\beta$  ratio of 6:1 for D-xylose as the immediate product from the SXA-catalyzed hydrolysis of X2 [3]; from the latter, it can be inferred that the reducing D-xylose moiety of X2 has an anomeric isomer ratio of 2.5:1 ( $\alpha$ : $\beta$ ). Left syringe of the stopped-flow contained 0.951, 1.90, or 9.51 mM 4NPA in 100 mM succinate–NaOH, pH 5.3 at 25°C. When the  $\alpha$ : $\beta$  ratio of D-xylose was 6:1, the right syringe contained 5.07  $\mu\text{M}$  SXA and 0, 8.6, or 17.2 mM X2 in 100 mM succinate–NaOH, pH 5.3 at 25°C. After 6 min preincubation to ensure complete conversion of X2 to D-xylose, reactions were initiated by injecting 50  $\mu\text{l}$  from each syringe through the mixing cuvette, and absorbance was recorded for 20 s at 360 nm to determine initial rates (fit to line). When the  $\alpha$ : $\beta$  ratio of D-xylose was 1:2.5, the right syringe contained 5.07  $\mu\text{M}$  SXA and 0, 20, or 40 mM D-xylose in 100 mM succinate–NaOH, pH 5.3 at 25°C. After 6 min preincubation (to mimic those containing X2), reactions were initiated by injecting 50  $\mu\text{l}$  from each syringe through the mixing cuvette, and absorbance was recorded for 20 s at 360 nm to determine initial rates (fit to line). For determination of steady-state kinetic parameters, initial rates were fitted to Eq. 2 (competitive inhibition).

For inhibition of SXA-catalyzed hydrolysis of 4NPX by 4NP, 1-ml reactions contained varied concentrations of 4NPX, 0 or 9.4 mM 4NP and 7.09–33.8 mM SXA (protomer) in 100 mM succinate–NaOH, pH 5.3 at 25°C. Before (time=0) and after (up to 6 min) initiating reactions by adding enzyme (7  $\mu\text{l}$  SXA in 20 mM sodium phosphate, pH 7.0), 100- $\mu\text{l}$  aliquots of reaction mixtures were removed and quenched with an equal volume of 0.2 M sodium phosphate pH 11.3 at 0°C, and diluted with 1 mM sodium phosphate, pH 10.5–11 (as above) before HPLC analysis. Concentrations of D-xylose produced vs time

were fitted to lines for determination of initial rates. For determination of steady-state kinetic parameters, initial rates were fitted to Eq. 2 (competitive inhibition).

### Equations

Data were fitted to equations by using the computer program Graft (Erithacus Software; Horley, UK) [15]. Symbol definitions for equations 1, 2, 3:  $\nu$  is the observed initial (steady-state) rate of catalysis,  $k_{\text{cat}}$  is the maximum rate of catalysis,  $S$  is the substrate concentration,  $K_m$  is the Michaelis constant,  $I$  is the inhibitor concentration,  $K_i$  is the dissociation constant for  $I$  from the EI complex, and  $K_{\text{is}}$  is the substrate dissociation constant from the EIS complex. For Eqs. 4, 5, 6, 7,  $p$  is the determined parameter at a single pH,  $P$  is the pH-independent value of the parameter,  $K_a$  is the acid dissociation constant of the group affecting  $P$ ,  $H^+$  is the proton concentration,  $K_{a1}$  is the acid dissociation constant of the first group affecting  $P$ ,  $K_{a2}$  is the acid dissociation constant of the second group affecting  $P$ ,  $P_1$  is the limit of  $p$  associated with  $K_{a1}$ , and  $P_2$  is the limit of  $p$  associated with  $K_{a2}$ .

$$\nu = \frac{k_{\text{cat}} * S}{K_m + S} \quad (1)$$

$$\nu = \frac{k_{\text{cat}} * S}{K_m \left(1 + \frac{I}{K_i}\right) + S} \quad (2)$$

$$\nu = \frac{k_{\text{cat}} * S}{K_m \left(1 + \frac{I}{K_i}\right) + S \left(1 + \frac{K_m * I}{K_{\text{is}} * K_i}\right)} \quad (3)$$

$$p = \frac{P}{1 + \frac{H^+}{K_a}} \quad (4)$$

$$p = \frac{P}{1 + \frac{K_a}{H^+}} \quad (5)$$

$$p = \frac{P}{1 + \frac{H^+}{K_{a1}} + \frac{K_{a2}}{H^+}} \quad (6)$$

$$p = \frac{P_1}{1 + \frac{H^+}{K_{a1}}} + \frac{P_2 - P_1}{1 + \frac{H^+}{K_{a2}}} \quad (7)$$

## Results and Discussion

An improved method for quenching SXA reactions was established for determination of steady-state kinetic parameters with xylooligosaccharide substrates X2–X6 (Table 1). The improved quenching method raises the pH of reaction mixtures to ~ pH 11, where SXA is inactive ( $pK_a=7$  for  $k_{cat}/K_m$ ) and lowers the temperature; it produces much lower background concentrations, stemming from hydrolysis of oligosaccharide substrates off the enzyme to D-xylose and smaller xylooligosaccharides, than the acid-quenching method employed previously [3], thus, allowing better estimations of rates, particularly at higher concentrations of substrate. In direct comparison to previous determinations at pH 5.3 and 25°C [3], the respective  $k_{cat}/K_m$  values for X2, X3, X4, X5, and X6 are lower by 9, 1, 12, 34, and 25% and the respective  $k_{cat}$  values are lower by 55, 45, 39, 49, and 15%. The lower  $k_{cat}$  values do not affect previous KINSIM simulations of reaction progressions for SXA-catalyzed hydrolysis of X4 and X6 (3) because initial X4 and X6 substrate concentrations of the reactions were low (30% of  $K_m$ ) where parameter  $k_{cat}/K_m$  governs rates, and as indicated, there are relatively small differences between the new and previously determined  $k_{cat}/K_m$  values. Also, SXA remains the most active  $\beta$ -xylosidase known for promoting hydrolysis of xylooligosaccharides with  $k_{cat}$  and  $k_{cat}/K_m$  values at pH 5.3 and 25°C that are higher than those of the second most active  $\beta$ -xylosidase known from the literature, the enzyme from *Bacillus pumilus* [16], determined at its pH optimum (pH 7.15) and 25°C, by factors of 10 (X2), 32 (X3), 31 (X4), 20 (X5), and 27 (X6) for  $k_{cat}$  and factors of 14 (X2), 16 (X3), 15 (X4), 10 (X5), and 13 (X6) for  $k_{cat}/K_m$ . For comparison,  $k_{cat}$  and  $k_{cat}/K_m$  values of SXA with substrate 4NPX at pH 5.3 and 25°C [3] are higher than those determined for the *B. pumilus* enzyme at pH 7.15 and 25°C [16] by factors of 4 and 5, respectively.

pH dependencies of SXA-catalyzed hydrolysis of X2 and X3 were determined using buffers of constant ionic strength ( $I=0.3$  M) from pH 4.3 to 9.2 (Figs. 2 and 3); denaturation of SXA at lower pH values precludes their analysis [2]. pH dependencies of  $k_{cat}$ ,  $k_{cat}/K_m$ , and  $1/K_m$  are similar in shape for X2 and X3, and similar  $pK_a$  values were determined (legends to Figs. 2 and 3). A small difference between the two substrates is that  $pK_a$  can be determined for the acidic limb of  $k_{cat}$  with X3 ( $pK_{a1}$  3.21), but no acidic limb is seen for  $k_{cat}$  with X2; the inability to determine the  $pK_a$  for X2 stems from the inability to analyze SXA kinetics below pH 4.3. Extension by 2 pH units of the  $pK_a$  for  $k_{cat}$  over that of  $k_{cat}/K_m$  ( $pK_{a1}$  4.8) would not be unusual [17]. Lower  $pK_a$  values for  $k_{cat}$  ( $pK_{a1}$  ~3.6) than  $k_{cat}/K_m$  ( $pK_{a1}$  ~5.0) for the acidic limbs are also seen with substrates 4NPX and 4NPA [3]. pH dependencies of  $1/K_m$  indicate that catalytically inactive, dianionic SXA ( $D14^-E186^-$ ) has 2.9-fold and 3.1-fold lower affinity than catalytically active, monoanionic SXA ( $D14^-E186^H$ ) for X2 and X3, respectively. In contrast,  $D14^-E186^-$  has 1.9-fold higher

**Table 1** Steady-state kinetic parameters of SXA acting on xylooligosaccharides<sup>a</sup>.

Substrate	$k_{cat}$ ( $s^{-1}$ )	$k_{cat}/K_m$ ( $mM^{-1} s^{-1}$ )	$K_m$ (mM)
1,4- $\beta$ -D-xylobiose (X2)	185 $\pm$ 3	90.2 $\pm$ 2.5	2.06 $\pm$ 0.08
1,4- $\beta$ -D-xylotriose (X3)	95.1 $\pm$ 1.5	44.8 $\pm$ 1.5	2.12 $\pm$ 0.10
1,4- $\beta$ -D-xylotetraose (X4)	91.6 $\pm$ 2.3	33.3 $\pm$ 2.0	2.75 $\pm$ 0.23
1,4- $\beta$ -D-xylopentaose (X5)	77.2 $\pm$ 3.6	27.0 $\pm$ 2.4	2.86 $\pm$ 0.38
1,4- $\beta$ -D-xylohexaose (X6)	81.5 $\pm$ 2.0	26.1 $\pm$ 1.2	3.12 $\pm$ 0.21

<sup>a</sup> Reactions contained varied concentrations of substrate in 100 mM succinate–NaOH, pH 5.3 at 25 °C. Initial-rate data were fitted to Eq. 1; SEs ( $\pm$ ) are indicated.

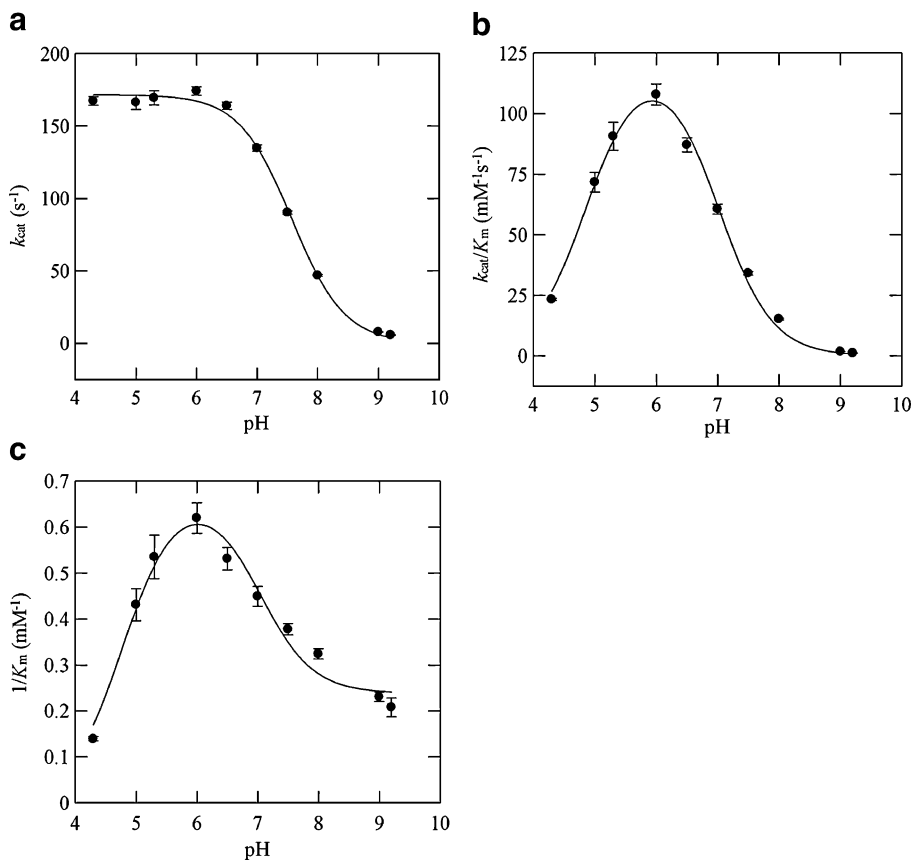


**Fig. 2** pH dependence of steady-state kinetic parameters for 1,4-β-D-xylobiose hydrolysis catalyzed by SXA at 25°C. Initial rates were determined from reactions in buffers of constant ionic strength ( $I=0.3$  M) and kinetic parameters were determined by fitting initial-rate data to Eq. 1; SEs ( $\pm$ ) are indicated. **a**  $k_{cat}$  vs pH. The curve was generated by fitting  $k_{cat}$  values vs pH to Eq. 5:  $pK_a=7.57\pm 0.03$ , pH-independent  $k_{cat}=172\pm 2$ . **b**  $k_{cat}/K_m$  vs pH. The curve was generated by fitting  $k_{cat}/K_m$  values vs pH to Eq. 6:  $pK_{a1}=4.86\pm 0.06$ ,  $pK_{a2}=7.01\pm 0.05$ , pH-independent  $k_{cat}/K_m=123\pm 5$ . **c**  $1/K_m$  vs pH. The curve was generated by fitting  $1/K_m$  values vs pH to Eq. 7:  $pK_{a1}=4.78\pm 0.11$ ,  $pK_{a2}=7.03\pm 0.17$ , middle limit  $1/K_m=0.682\pm 0.048$ , upper limit  $1/K_m=0.238\pm 0.022$

affinity than catalytically active, monoanionic SXA (D14<sup>-</sup>E186<sup>H</sup>) for 4NPX, and D14<sup>-</sup>E186<sup>-</sup> has no affinity for 4NPA [3].

Inhibition of SXA-catalyzed hydrolysis of 4NPX by D-xylose was determined at pH 5.3 and 25°C by using a continuous spectrophotometric method:  $K_i^{D\text{-xylose}}$  of  $9.63\pm 0.30$  mM and  $K_{is}^{D\text{-xylose}\cdot 4NPX}$  of  $15.9\pm 2.1$  mM were determined by fitting the data to Eq. 3, describing noncompetitive (or “mixed”) inhibition. For comparison with actual reaction progression data acquired by following production of 4NP spectroscopically, values of  $k_{cat}^{4NPX}$  ( $32.1\pm 0.5$ ),  $K_m^{4NPX}$  ( $0.716\pm 0.032$ ),  $K_i^{D\text{-xylose}}$  ( $9.63\pm 0.30$  mM), and  $K_{is}^{D\text{-xylose}\cdot 4NPX}$  ( $15.9\pm 2.1$  mM) were used as inputs to KINSIM for simulations of four reaction progressions of SXA-catalyzed hydrolysis of 1 mM 4NPX and 5 mM 4NPX at pH 5.3 and 25°C (Fig. 4). Whereas the simulations adequately describe the two progressions at 1 mM 4NPX, the simulations fail to account for the production of 4NP towards the end of 4NPX consumption of the two progressions containing 5 mM 4NPX. Two possibilities, which could rationalize the

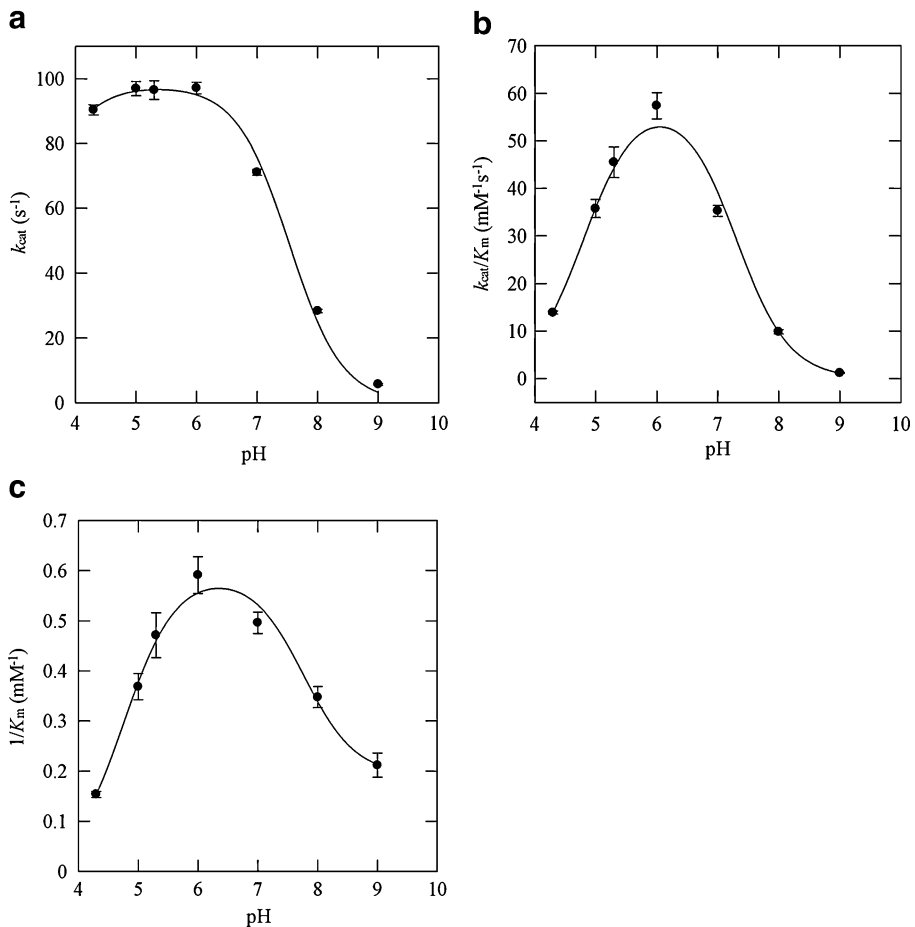


**Fig. 3** pH dependence of steady-state kinetic parameters for 1,4- $\beta$ -D-xylotriose hydrolysis catalyzed by SXA at 25°C. Initial rates were determined from reactions in buffers of constant ionic strength ( $I=0.3$  M), and kinetic parameters were determined by fitting initial-rate data to Eq. 1; SEs ( $\pm$ ) are indicated. **a**  $k_{cat}$  vs pH. The curve was generated by fitting  $k_{cat}$  values vs pH to Eq. 6:  $pK_{a1}=3.21\pm 0.27$ ,  $pK_{a2}=7.53\pm 0.06$ , pH-independent  $k_{cat}=98.0\pm 2.3$ . **b**  $k_{cat}/K_m$  vs pH. The curve was generated by fitting  $k_{cat}/K_m$  values vs pH to Eq. 6:  $pK_{a1}=4.80\pm 0.06$ ,  $pK_{a2}=7.30\pm 0.04$ , pH-independent  $k_{cat}/K_m=58.9\pm 3.3$   $mM^{-1} s^{-1}$ . **c**  $1/K_m$  vs pH. The curve was generated by fitting  $1/K_m$  values vs pH to Eq. 7:  $pK_{a1}=4.76\pm 0.05$ ,  $pK_{a2}=7.76\pm 0.14$ , middle limit  $1/K_m=0.594\pm 0.027$ , upper limit  $1/K_m=0.191\pm 0.017$

discrepancies, were addressed experimentally. The first of these is that the  $K_i^{D\text{-xylose}}$  (9.63 mM) input of the simulation was determined from inhibition studies with D-xylose, predominantly in the  $\beta$  conformation ( $\alpha:\beta$  ratio of 1:2.5 at equilibrium), whereas the product of SXA-catalyzed hydrolysis of 4NPX is temporally in the  $\alpha$  conformation (half life~1 h) before mutarotation establishes equilibrium favoring the  $\beta$  conformation [3]; potentially,  $\alpha$ -D-xylose has greater affinity than  $\beta$ -D-xylose for SXA. To address this, X2 was preincubated with SXA for 6 min to fully convert to D-xylose with  $\alpha:\beta$  ratio of 6:1 [3] before initiating reactions with varied concentrations of 4NPA for determination of  $K_i^{D\text{-xylose}}$  to compare with  $K_i^{D\text{-xylose}}$ , determined from reactions with SXA preincubated with D-xylose ( $\alpha:\beta$  ratio of 1:2.5) before initiating reactions with varied concentrations of 4NPA. In contrast to 4NPX, SXA-catalyzed hydrolysis of 4NPA is competitively inhibited by D-xylose. From the data collected with D-xylose ( $\alpha:\beta$

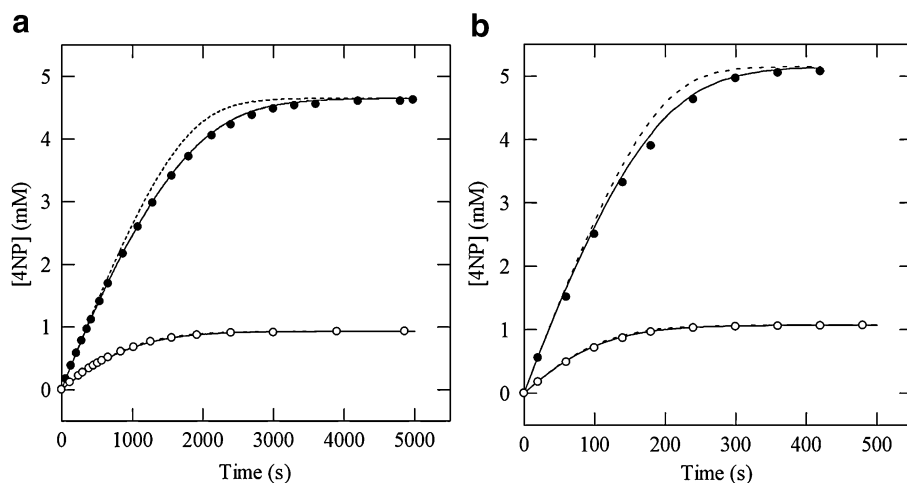


**Fig. 4** Progress curves of 4NPX hydrolysis catalyzed by SXA. Reactions contained 100 mM succinate–NaOH, pH 5.3 at 25°C. [4NP] was determined spectrophotometrically. Curves were generated from the KINSIM calculations, assuming rapid equilibrium binding, with the indicated [enzyme] and [4NPX] and the following as inputs:  $E+S \rightleftharpoons E\cdot S$  ( $K_m^{4NPX}=0.716\pm 0.032$  mM);  $E\cdot S \rightarrow E+P+Q$  ( $k_{cat}^{4NPX}=32.1\pm 0.5$  s<sup>-1</sup>);  $E\cdot P \rightleftharpoons E+P$  ( $K_i^{D\text{-xylose}}=9.63\pm 0.30$  mM);  $E\cdot Q \rightleftharpoons E+Q$  ( $K_i^{4NP}=6.28\pm 0.55$  mM);  $EP\cdot 4NPX \rightleftharpoons EP+4NPX$  ( $K_{is}^{D\text{-xylose}\cdot 4NPX}=15.9\pm 2.1$  mM). *Solid curves* included all parameters as inputs in the KINSIM simulations; *dotted curves* excluded the  $K_i^{4NP}$  term in the simulations. **a** Reactions were initiated by addition of enzyme to give initial reaction conditions of 52 nM SXA and 0.93 mM 4NPX (*empty circles*) or 104 nM SXA and 4.65 mM 4NPX (*filled circles*). **b** Reactions were initiated by addition of enzyme to give initial reaction conditions of 520 nM SXA and 1.07 mM 4NPX (*empty circles*) or 1040 nM SXA and 5.15 mM 4NPX (*filled circles*)

ratio of 6:1),  $K_i^{D\text{-xylose}}$  of  $11.9\pm 0.3$  was determined (Fig. 5a). From the data collected with D-xylose ( $\alpha:\beta$  ratio of 1:2.5),  $K_i^{D\text{-xylose}}$  of  $11.8\pm 0.3$  was determined (Fig. 5b). If, for example, all inhibitory activity resided in the  $\alpha$  anomeric isomer and  $\beta$ -D-xylose had no affinity for SXA, then  $K_i^{D\text{-xylose}}$  for D-xylose with  $\alpha:\beta$  ratio of 1:2.5 would be threefold that for D-xylose with  $\alpha:\beta$  ratio of 6:1. Therefore, the two anomeric isomers of D-xylose possess similar affinities for SXA, and corrections, on the basis of  $\alpha$  and  $\beta$  content, cannot account for the overestimation of reaction progress by the simulations in comparison to the actual progressions of Fig. 4. Similarly, from stopped-flow reactions at pH 7.0 (100 mM sodium phosphate, adjusted with NaCl to ionic strength of 0.3 M) and 25°C,  $K_i^{D\text{-xylose}}$  values for inhibition of SXA-catalyzed hydrolysis of 4NPA were similar when the D-xylose solutions contained  $\alpha:\beta$  anomeric isomer ratios of 1:2.5 ( $K_i^{D\text{-xylose}}=5.15\pm 0.08$  mM) or 6:1 ( $K_i^{D\text{-xylose}}=4.97\pm 0.05$  mM).

The second possible cause for discrepancies between the simulated and actual progressions is the unaccounted for potential of product 4NP to inhibit the SXA-catalyzed hydrolysis of 4NPX. To address this,  $K_i^{4NP}$  for inhibition of SXA-catalyzed hydrolysis of 4NPX was determined at pH 5.3 and 25°C by using HPLC analysis of D-xylose produced from 4NPX to determine catalyzed rates in the absence and presence of 4NP and fitting the rate data to Eq. 2, describing competitive inhibition (Fig. 6). By including the determined value of  $K_i^{4NP}$  ( $6.28\pm 0.55$  mM) in the simulations of SXA-catalyzed hydrolysis of 4NPX, better agreement with actual reaction progressions is generated (Fig. 4).

For comparison with actual reaction progress data acquired by HPLC quantification of D-xylose and 1,4- $\beta$ -D-xylobiose (X2) concentrations, steady-state values for  $k_{cat}^{X2}$  ( $185\pm 3$  s<sup>-1</sup>),  $K_m^{X2}$  ( $2.06\pm 0.08$  mM) and  $K_i^{D\text{-xylose}}$  ( $9.63\pm 0.30$  mM) were used for KINSIM inputs for simulations of SXA-catalyzed reactions containing 0.922 mM X2 and 7.31 mM X2 (Fig. 7).

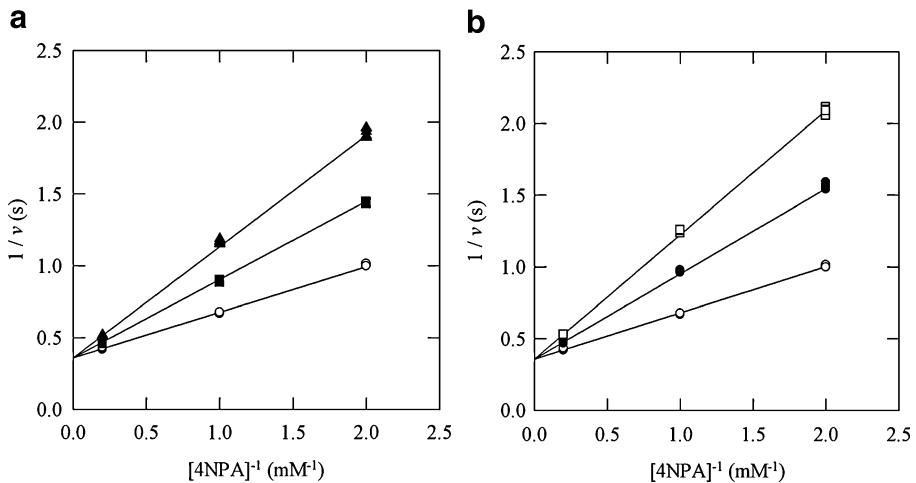
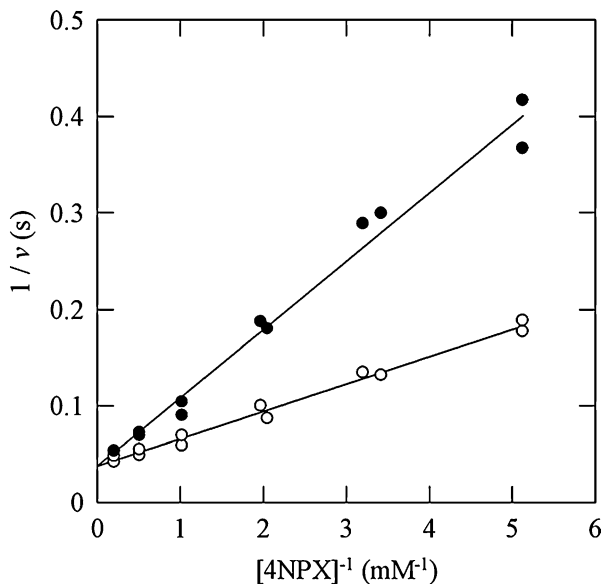


**Fig. 5** Influence of D-xylose anomeric stereochemistry on inhibition of SXA-catalyzed hydrolysis of 4NPA at pH 5.3 and 25°C. Left syringe of stopped-flow instrument contained varied 4NPA concentrations in 100 mM succinate–NaOH, pH 5.3 at 25°C. Right syringe contained the indicated concentrations of SXA and D-xylose (or 1,4- $\beta$ -D-xylobiose) in 100 mM succinate–NaOH, pH 5.3 and 25°C. Contents of the syringes were preincubated 6 min at 25°C, to achieve full conversion of 1,4- $\beta$ -D-xylobiose to D-xylose, before initiating 20-s reactions (by mixing 50  $\mu$ l from each syringe) and recording linear absorbance changes at 360 nm for determination of initial rates ( $v$  in moles 4NP produced per second per mole SXA protomer). **a** D-Xylose  $\alpha$ : $\beta$  ratio of 6:1. Right syringe of stopped flow contained 5.07  $\mu$ M SXA, and the following concentrations of 1,4- $\beta$ -D-xylobiose: 0 (empty circles), 8.6 mM (filled squares), and 17.2 mM (filled triangles). Lines were generated by fitting initial rate data to Eq. 2 (competitive inhibition):  $K_i^{\text{D-xylose}}=11.9\pm 0.3$  mM,  $k_{\text{cat}}^{4\text{NPA}}=2.78\pm 0.01$  s $^{-1}$ ,  $k_{\text{cat}}/K_m^{4\text{NPA}}=3.16\pm 0.04$  mM $^{-1}$  s $^{-1}$ , and  $K_m^{4\text{NPA}}=0.880\pm 0.13$  mM. **b** D-Xylose  $\alpha$ : $\beta$  ratio of 1:2.5. Right syringe of stopped flow contained 5.07  $\mu$ M SXA, and the following concentrations of D-xylose: 0 (empty circles), 20 mM (filled circles), 40 mM (empty squares). Lines were generated by fitting initial rate data to Eq. 2 (competitive inhibition):  $K_i^{\text{D-xylose}}=11.8\pm 0.3$  mM,  $k_{\text{cat}}^{4\text{NPA}}=2.79\pm 0.01$  s $^{-1}$ ,  $k_{\text{cat}}/K_m^{4\text{NPA}}=3.10\pm 0.04$  mM $^{-1}$  s $^{-1}$ , and  $K_m^{4\text{NPA}}=0.900\pm 0.013$  mM

**Fig. 6** Inhibition of SXA-catalyzed hydrolysis of 4NPX by 4-nitrophenol (4NP) at pH 5.3 and 25°C. Reactions contained 0 (empty circles) or 9.4 mM 4NP (filled circles), 7.09–33.8 nm SXA, and varied concentrations of 4NPX in 100 mM succinate–NaOH, pH 5.3 at 25°C. Concentrations of D-xylose produced were quantified by HPLC for determination of initial rates ( $v$ ). Lines were generated by fitting initial rates to Eq. 2 (competitive inhibition):  $K_i^{4\text{NP}}=6.28\pm 0.55$  mM,  $k_{\text{cat}}^{4\text{NPX}}=26.7\pm 1.1$  s $^{-1}$ , and  $K_m^{4\text{NPX}}=0.758\pm 0.059$  mM



The simulations adequately describe reaction progress at both high and low X2 concentrations, conditions where the  $K_i^{D\text{-xylose}}$  term is more and less important, respectively, to the calculations. Thus, the xylobiose reactions substantiate that  $\alpha$  and  $\beta$  anomeric conformations of D-xylose have similar affinities for SXA.

## Conclusions

The small discrepancies between the actual and simulated (when not including  $K_i^{4NP}$  in the calculations) progress curves for SXA-catalyzed hydrolysis of 4NPX (Fig. 4) prompted experiments to determine  $K_i$  values for 4NP and the two preparations of D-xylose with different anomeric isomer ratios. Determinations that the two anomeric isomers of D-xylose have similar  $K_i$  values and that 4NP binds to SXA and inhibits catalysis allow more accurate predictions of SXA-catalyzed reactions (Figs. 4 and 7). Of course the absence of complicating factors, such as subunit cooperativity (SXA is a homotetramer) and transglycosylation back reactions, simplify the parameters needed for kinetic simulations. The ability to simulate reaction progress could have utility in engineering saccharification processes. Undoubtedly, the lack of complicating factors (cooperativity, transglycosylation), which lower rates of hydrolysis, favors the effectiveness of SXA in saccharification processes.

Based on the twofold tighter binding of 4NPX by the catalytically inactive, dianionic SXA ( $D14^-E186^-$ ) than by the catalytically active, monoanionic SXA ( $D14^-E186^H$ ), it might have been projected that X2 and X3 would share this property of forming relatively high-affinity, dead-end complexes, which would be detrimental to the usefulness of SXA at

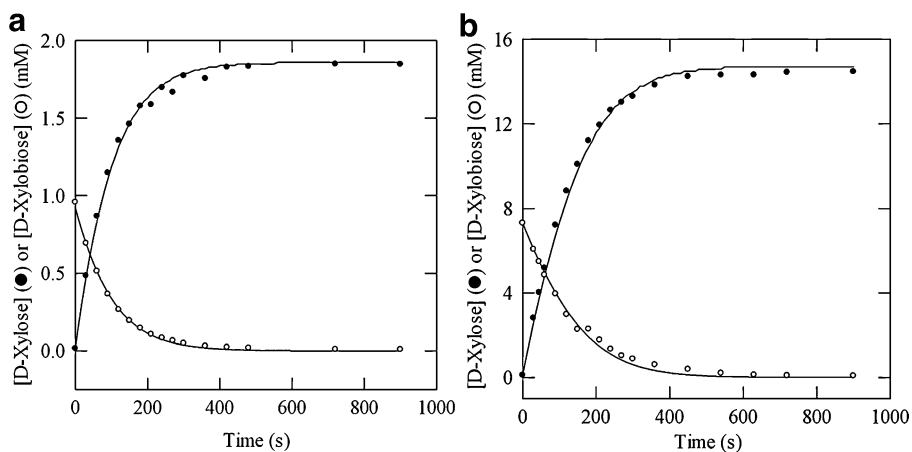


**Fig. 7** Progress curves of 1,4- $\beta$ -D-xylobiose (X2) hydrolysis catalyzed by SXA. Reactions contained 100 mM succinate-NaOH, pH 5.3 at 25 °C. Curves were generated from the KINSIM calculations, assuming rapid equilibrium binding, with the indicated [enzyme] and [X2] and the following as inputs:  $E + X2 \rightleftharpoons E \cdot X2$  ( $K_m = 2.06 \pm 0.08$  mM);  $E \cdot X2 \Rightarrow E + X1 + X1$  ( $k_{cat}^{X2} = 185 \pm 3$  s $^{-1}$ );  $E \cdot X1 \rightleftharpoons E + X1$  ( $K_i^{D\text{-xylose}} = 9.63 \pm 0.32$  mM). Determined  $K_m^{X2}$  and  $k_{cat}^{X2}$  values at pH 5.3 at 25 °C are from Table 1, and determination of  $K_i^{D\text{-xylose}}$  at pH 5.3 at 25 °C is described in the text. **a** Reaction contained 152 nM SXA, 0.922 mM X2, and 0.0146 mM X1 (contaminant of X2); concentrations of X1 (filled circles) and X2 (empty circles) were monitored by HPLC. **b** Reaction contained 303 nM SXA, 7.31 mM X2, and 0.111 mM X1 (contaminant of X2); concentrations of X1 (filled circles) and X2 (empty circles) were monitored by HPLC

higher pH. Determination of threefold weaker binding of X2 and X3 by D14<sup>-</sup>E186<sup>-</sup> than by D14<sup>-</sup>E186<sup>H</sup> favors the effectiveness of SXA as a catalyst.

**Acknowledgments** I thank Jay D Braker for excellent technical assistance in contributing to this work.

## References

1. Whitehead, T. R., & Cotta, M. A. (2001). *Current Microbiology*, *43*, 293–298.
2. Jordan, D. B., Li, X-L., Dunlap, C. A., Whitehead, T. R., & Cotta, M. A. (2007). *Applied Biochemistry and Biotechnology*, *137-140*, 93–104.
3. Jordan, D. B., Li, X-L., Dunlap, C. A., Whitehead, T. R., & Cotta, M. A. (2007). *Applied Biochemistry and Biotechnology*, *141*, 51–76.
4. Henrissat, B. (1991). *Biochemistry Journal*, *280*, 309–316.
5. Henrissat, B., & Davies, G. J. (1997). *Current Opinion in Structural Biology*, *7*, 637–644.
6. Saha, B. C. (2003). *Journal of Industrial Microbiology & Biotechnology*, *30*, 279–291.
7. Saha, B. C. (2000). *Biotechnology Advances*, *18*, 403–423.
8. Gray, K. A., Zhao, L., & Emptage, M. (2006). *Current Opinion in Chemical Biology*, *10*, 141–146.
9. Shallom, D., & Shoham, Y. (2003). *Current Opinion in Microbiology*, *6*, 219–228.
10. Brück, C., Ben-David, A., Shallom-Shezifi, D., Leon, M., Niefind, K., Shoham, G., et al. (2006). *Journal of Molecular Biology*, *359*, 97–109.
11. Jordan, D. B., & Braker, J. D. (2007). *Archives of Biochemistry and Biophysics*, *465*, 231–246.
12. Gill, S. C., & von Hippel, P. H. (1989). *Analytical Biochemistry*, *182*, 319–326.
13. Barshop, B. A., Wrenn, R. F., & Frieden, C. (1983). *Analytical Biochemistry*, *130*, 134–145.
14. Kezdy, F. J., & Bender, M. L. (1962). *Biochemistry*, *1*, 1097–1106.
15. Leatherbarrow, R. J. (2001). *Grafit Version 5*, Erithacus Software Ltd., Horley, U.K.
16. Van Doorslaer, E., Kersters-Hilderson, H., & De Bruyne, C. K. (1985). *Carbohydrate Research*, *140*, 342–346.
17. Cleland, W. W. (1982). *Methods in Enzymology*, *87*, 390–405.

Supplied by the U.S. Department of Agriculture, National Center for Agricultural Utilization Research, Peoria, Illinois